# Appropriate Modeling of the Ear for Compliance Testing of Handheld MTE with SAR Safety Limits at 900/1800 MHz

Michael Burkhardt, *Member, IEEE,* and Niels Kuster, *Member, IEEE*

***Abstract*—A variety of phantoms simulating the human head have been used to test compliance of mobile telecommunications equipment with safety standards. Whereas numerical compliance procedures have mostly been performed using complex anatomical phantoms based on magnetic resonance imaging (MRI) data, experimental procedures have mainly relied on homogeneous phantoms, the ears of which have often been modeled as lossless spacers. Previous studies had indeed demonstrated that the absorption in the head tissue, except the outer ear, can be well represented by a homogeneous head of appropriate shape and material. The objectives of this paper were to fill the gap of the remaining open issues, namely: to evaluate the exposure in the ear region with respect to the spatial-peak specific absorption rate and to evaluate the most appropriate modeling of the ear for experimental evaluations such that it represents the maximum exposure of a reasonable cross section of cellular phone users. This paper is based on a detailed numerical phantom produced using high-resolution MRI scans. During scanning, the ear was naturally collapsed as it occurs when using a cellular phone. The results of this study lead to the conclusion that the spatial-peak absorption occurring in the inner and outer ear can be reliably modeled either by a lossless spacer of not thicker than 3–4 mm or by partially filling the simulated pinna with head tissue simulating media, whereas the minimum distance between the device and liquid should not be larger than 3 mm.**

***Index Terms*—Compliance testing, dosimetry, ear modeling, handheld mobile telecommunications equipment.**

## I. Introduction

REGULATORY bodies in the U.S. [1], Europe [2], and Japan [3] require compliance testing of handheld mobile communications equipment prior to market introduction. For example, [2] requires that demonstration of compliance must be shown for a reasonable cross-section of mobile telecommunications equipment (MTE) users in four different operational conditions and for all device configurations, whereby the uncertainty must be added to the results. Devices with antenna input powers of less than 20 mW are excluded. Many compliance tests of handheld devices have been performed experimentally using measurement systems similar to the one described in [4]. Although multitissue phantoms have been developed [5], demonstration of compliance can only be performed based on homogeneous head phantoms, since the entire volume must be accessible by the probe. In most cases, the ear has been replaced by a lossless spacer [4], [6], [7]. The suitability of homogeneous phantoms for exposure evaluations had been demonstrated based on the results of a series of studies [8]–[11] systematically investigating the dependence of the absorption on the internal anatomy. The objective of another study [7] was to experimentally evaluate the head shape in the vicinity of the ear as well as the thickness of the collapsed ear. The study was performed with 52 male and female volunteers. Based on this data, a phantom was proposed for compliance testing, the shape of which corresponds to the 90% percentile of greatest absorption for the evaluated group. Following the same approach, it was suggested that the ear should be modeled by a lossless spacer of 4 mm, corresponding to the 10% percentile. Although it was noted that there is absorption in the pinna, it was argued that the losses in the outer ear would be compensated by the replacement of the low-loss structure of the inner ear (bony structure with air cavities) through the lossy tissue simulating material. However, this argument was based on rational reasoning rather than on hard scientific facts. Providing similar arguments, some groups have used the same phantom, but increased the distance to 6 mm, which approximately represents the average thickness of the collapsed ear.

The lossless spacer has always been criticized since it does not account for the losses in the pinna, which might be quite large due to the close proximity of this tissue to parts of the phone, potentially conducting significant RF currents. This criticism was supported by data obtained from numerical studies based on inhomogeneous head phantoms derived from magnetic resonance images (MRI), which showed greatly enhanced specific absorption rate (SAR) values in the external ear [12]–[14]. However, all these studies were performed based on phantoms with noncollapsed ears, which obviously overestimates the ratio between energy absorbed in the ear and the rest of the head. In addition, the maximum voxel sizes were rather large (up to 15 $mm^3$), which may result in significant overestimation of the exposure due to numerical artifacts [15].

Nevertheless, there was a clear need to thoroughly address the question regarding the appropriate modeling of the ear for compliance testing. The objective of this study was to evaluate the exposure in the ear region based on a high-resolution phantom with an accurate model of a collapsed ear and to investigate possibilities for appropriate modeling of the ear in experimental setups, which neither greatly overestimate nor underestimate the actual user exposure.

Manuscript received June 22, 1999. The work was supported by T-Mobil GmbH, by Swisscom, by the Swiss Priority Research Program MINAST, by the EUREKA Project SARSYS, and by Schmid & Partner Engineering AG.

M. Burkhardt is with the Regulatory Group, diAx, Zurich, Switzerland.

N. Kuster is with the Swiss Federal Institute of Technology (ETH), CH-8092 Zurich, Switzerland.

Publisher Item Identifier S 0018-9480(00)09544-2.

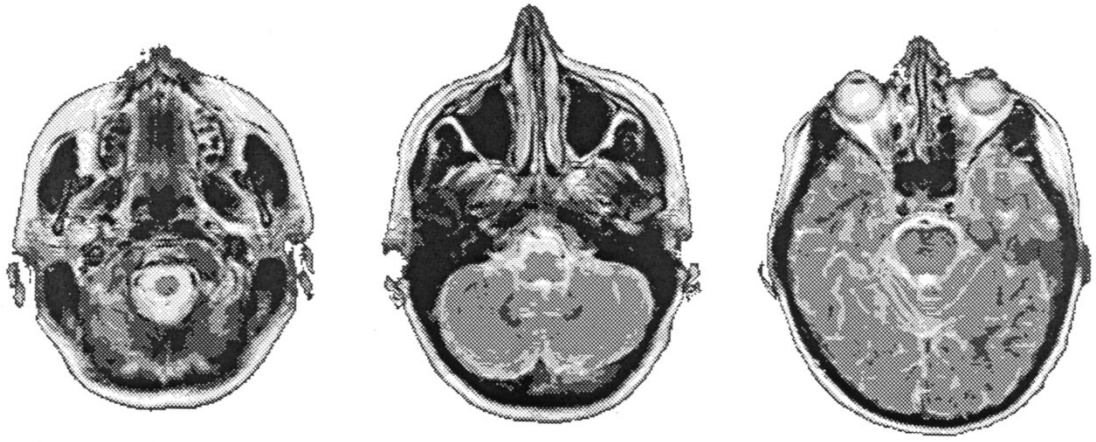

Fig. 1. MRI slices at three different locations in the ear region. The ears had been gently pressed toward the head as it would occur in a real-world MTE user situation.

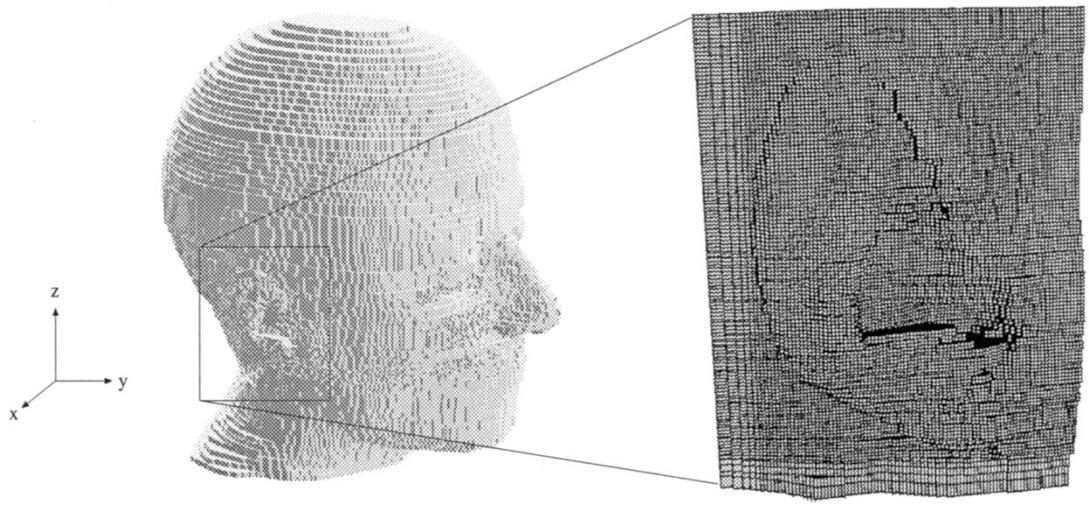


Fig. 2. Voxel model of the head (left-hand side) and a close-up view of the high-resolution ear region (right-hand side).

## II. Head Modeling and Transmitter Representation

The MRI data sets from which our previous phantoms were derived were taken without collapsing the ear, nor did they provide the necessary resolution for accurate modeling of the ear region. For the purpose of this study, a high-resolution MRI data set of the complete head of a healthy female volunteer (age 40) was obtained from the University Hospital of Zurich, Zurich, Switerland. The ears were gently pressed to the head surface in order to obtain the appropriate ear shape for a realistic MTE user situation (Fig. 1). The MRI slices were separated by 1 mm in the ear region and 3 mm in the upper and lower head regions. From this data, a computer-aided design (CAD) model was constructed consisting of 121 slices, which were separated into 12 different tissue types. Two different numerical phantoms were created: 1) a high-resolution model with 0.125-mm$^3$ voxels in the ear region and expanding mesh steps in the upper and lower head regions and 2) a model with 1-mm$^3$ voxels in the ear region and 9-mm$^3$ voxels in the upper and lower head regions for fast parametric studies. A detailed view of the high-resolution ear region is given in Fig. 2. The model with the highest resolution required a computational domain of approximately 14 million voxels and 1.2 Gbytes of memory, and took approximately 60 h for ten periods on a Sun Ultra 2 (300 MHz) computer.

Additionally, a homogeneous phantom was created by cutting the ear away in all MRI slices and smoothing the head surface in the ear region. The air-containing auditory canal was filled with tissue. All tissues were simulated with the same dielectric parameter sets of HTSL1 and HTSL2, as given in Table I. HTSL1 corresponds to the values used in our previous studies [9]–[11] and HTSL2 was initially proposed by the Federal Communications Commission (FCC) and approximately corresponds to the arithmetic average of grey and white matter.

In order to comprehensively study the exposure of the ear region, two different generic transmitters were used: 1) a 0.45-$\lambda$ dipole and 2) a generic phone (Fig. 3). The basic study was performed using the dipole. In order to validate the generality of the findings for other transmitters, additional simulations were performed with a generic phone in various positions.

## III. Methods

The study was performed by employing the finite-difference time-domain (FDTD) technique, applying a three-dimensional

TABLE I
DIELECTRIC PARAMETER SETS OF THE HEAD TISSUE SIMULATING LIQUIDS (HTSL) USED FOR THE HOMOGENEOUS HEAD MODELING

| tissue | Spec. gravity $\rho[g/cm^3]$ | 900 MHz $\epsilon_r$ | 900 MHz $\sigma[mho/m]$ | 1800 MHz $\epsilon_r$ | 1800 MHz $\sigma[mho/m]$ |
|---|---|---|---|---|---|
| HTSL1: Head Tissue Simulating Media | 1.00 | 43.5 | 0.90 | 41.0 | 1.69 |
| HTSL2: Average Brain (FCC) | 1.00 | 45.8 | 0.77 | 43.5 | 1.15 |

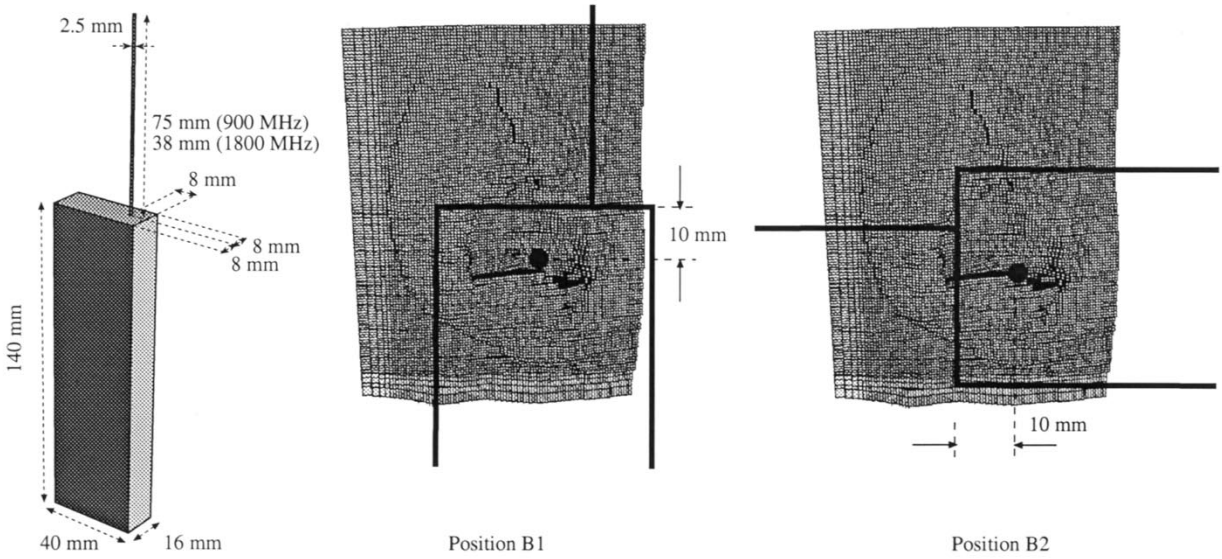


Fig. 3. Dimensions of the metal case of the generic phone (left-hand side) and vertical ($B1$) and horizontal ($B2$) phone positions (right-hand side). The metallic box is at a distance of 2 mm from the outermost voxel of the pinna, corresponding to a 2-mm plastic layer covering the metal case. The dot corresponds to the location of the opening of the auditory canal.

(3-D) in-house kernel developed within the framework of a Swiss priority research program. For the numerical model, an inhomogeneous grid with expanding mesh steps was used to minimize memory costs and computation time. The time step was chosen according to the Courant limit [16]. Second-order Mur absorbing boundary conditions (ABCs) were used for these calculations to truncate the computational domain despite the availability of other ABCs in the current implementation, including a Higdon operator up to fourth order and perfectly matched layer (PML). This enables some computational expenses to be saved since scattering at nonperfectly absorbing boundaries is of negligible significance for close near-field studies due to the strong dependence of the absorption on the distance [8]. The head models for validation purposes have been simulated with the FDTD–similar finite-integration (FI) implementation applying the commercially available software package MAFIA [17]. Details on the FDTD technique can be found in [16] and in [18] for FI.

A computer-aided design (CAD) tool (SEMCAD, Schmid & Partner Engineering AG, Zurich, Switzerland) was used for the import of CAD data derived from the MRI images, for the rotation of the CAD data and the subsequent automatic discretization. The rotation of the CAD data prior to discretization is necessary to obtain reliable tilted head models, as used in this paper.

The excitation of the dipole and generic phone exposure was chosen to be an added source [19] in order to directly normalize all values to the feedpoint current. This approach is advantageous since the SAR is predominantly induced by the $H$-field, which is directly proportional to the feedpoint current [8]. SAR values were calculated in the center of the voxels by interpolating all 12 electric-field values of the surrounding edges.

The 1-g/10-g spatial-peak SAR values were calculated by expanding a cube at each grid point until the desired mass was reached. The cube was always aligned parallel to the grid coordinates and each outermost layer of the cube consisted of at least one voxel of tissue, i.e., the cube not only contained tissue, but also air voxels. This evaluation approach is in good agreement with the latest definition for the "cube" described in the various standards.

The experimental data used for validation purposes was obtained using DASY3 (Schmid & Partner Engineering AG), which is the successor of the dosimetric assessment scanner described in [4] and provides enhanced precision and flexibility.

## IV. VALIDATION OF THE NEW HEAD MODEL

In the first step, the performance of the new phantom was compared with those of the previous phantoms (Fig. 4). A comprehensive data set is available for the excitation of a 0.45-$\lambda$ dipole source at 900 MHz. The orientation of the dipole is vertical and the position of the feedpoint is 5 mm above the pinna and at a distance of 15 mm between the feedpoint and surface of the head. The same dielectric parameter set as in the previous studies was chosen, which corresponds to the Dielectric Database from Microwave Consultants, London, U.K. [20]. The SAR distribution and spatial-peak SAR values were computed

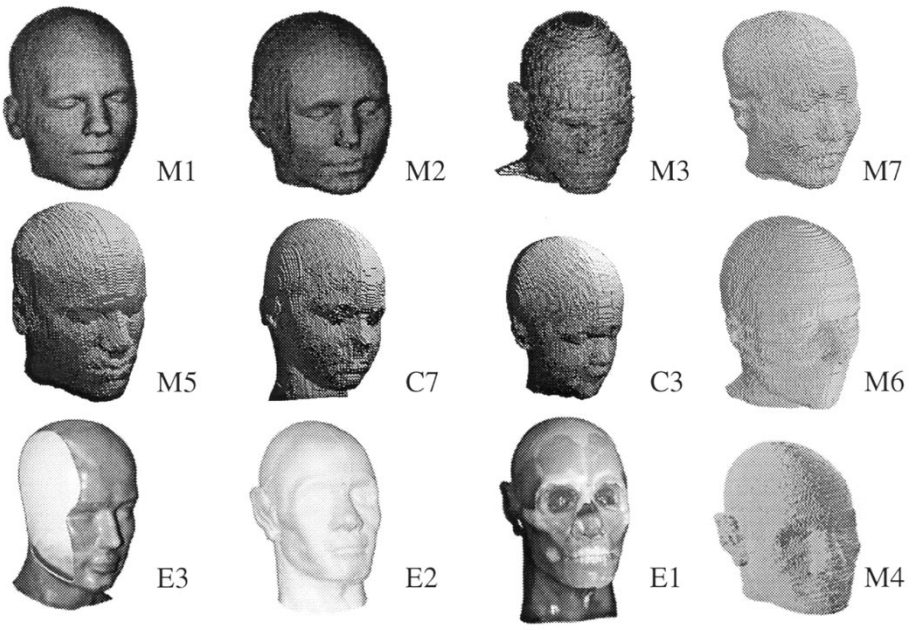


Fig. 4. Head phantom database used in previous studies. Numerical head phantoms based on MRI data: male head phantoms evaluated in [9]–[11] ($M1$, $M2$, $M3$, $M5$), Asian male head ($M7$), which has not yet been studied, seven- ($C7$) and three-year-old ($C3$) children evaluated in [11], new female head with collapsed ears ($M6$). Experimental head phantoms: shell phantom for compliance testing described in [9] ($E3$), shell phantom ($E2$) with the same head shape as $E1$, a five-tissue phantom described in [5]. $M4$ is the numerical model of $E1$, based on CT scans.

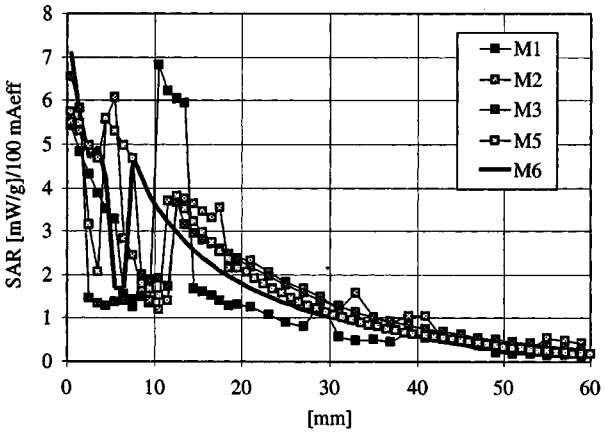


Fig. 5. SAR distribution along a line perpendicular to the axis of a 0.45-$\lambda$ (900-MHz) dipole directly behind the feedpoint for five inhomogeneous MRI-based head phantoms. The dipole is located with its feedpoint 5 mm above the pinna, at a distance of 15 mm to the surface of the head.

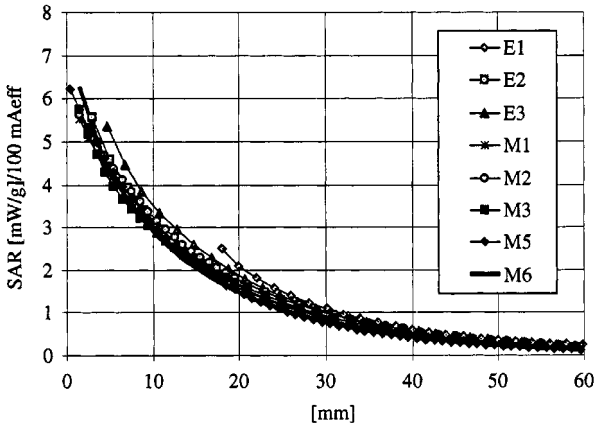


Fig. 6. Comparison of the SAR distribution for the same excitation and phantoms ($M1, \ldots, M6$) than in the previous figure, but for which the dielectric parameters of all tissues were replaced by $\epsilon_{r1} = 43.5$, $\sigma_1 = 0.9$ mho/m, and $\rho = 1$ g/cm$^3$. In addition, the experimental values for three experimental head phantoms ($E1$, $E2$, and $E3$) are given.

for the inhomogeneous phantom, as well as for the homogeneous phantom in which the dielectric parameters of all tissues were replaced by the parameters of the head tissue simulating liquid (HTSL1).

The SAR distributions along a line perpendicular to the dipole axis directly behind the feedpoint are compared in Figs. 5 and 6. In Fig. 6, the experimental data for the three different head phantoms $E1/E2/E3$ (see Fig. 4) have been added. In Fig. 7, the 1- and 10-g spatial-peak SAR values are compared.

The obtained SAR data for the new head model is well within the given range of the other head models (Figs. 5 and 6), verifying the previous conclusions that local absorption is strongly dependent on differences of the internal anatomy, whereas the spatial-peak SAR values vary only within a small

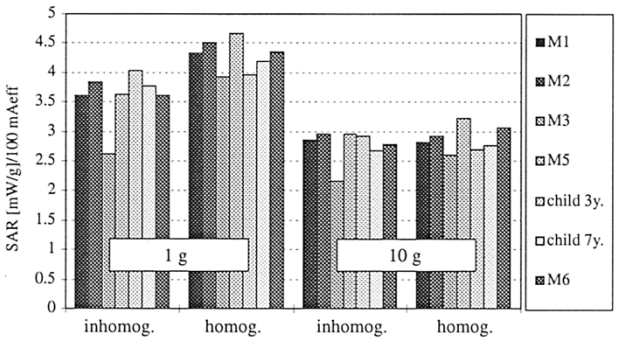


Fig. 7. Comparison of the spatial-peak SAR values averaged over 1- and 10-g for the five phantoms $M1, \ldots, M6$ and the two children phantoms $C7$ and $C3$.

TABLE II
DIELECTRIC PARAMETERS AT 900 AND 1800 MHz [21] AND TISSUE DENSITIES [14]

| tissue | Spec. gravity $\rho[g/cm^3]$ | 900 MHz $\epsilon_r$ | 900 MHz $\sigma[mho/m]$ | 1800 MHz $\epsilon_r$ | 1800 MHz $\sigma[mho/m]$ |
|---|---|---|---|---|---|
| bone | 1.81 | 20.8 | 0.34 | 19.3 | 0.59 |
| skin | 1.01 | 43.7 | 0.86 | 41.4 | 1.21 |
| fat | 0.92 | 11.3 | 0.11 | 11.0 | 0.19 |
| muscle | 1.04 | 56.0 | 0.97 | 54.4 | 1.39 |
| brain | 1.04 | 45.8 | 0.77 | 43.5 | 1.15 |
| CSF | 1.01 | 68.6 | 2.41 | 67.2 | 2.92 |
| blood | 1.06 | 61.4 | 1.54 | 59.4 | 2.04 |
| cartilage | 1.10 | 42.7 | 0.78 | 40.2 | 1.29 |
| eye: | | | | | |
| vitreous humour | 1.01 | 68.9 | 1.64 | 68.6 | 2.03 |
| lens | 1.10 | 46.6 | 0.79 | 45.4 | 1.15 |
| sclera | 1.17 | 55.3 | 1.17 | 53.6 | 1.60 |
| air | 0.00 | 1.0 | 0.00 | 1.0 | 0.00 |

range (Fig. 7). In other words, the spatial-peak SAR—at least for the area above the ear—can be well assessed using a homogeneous phantom having the appropriate dielectric parameters.

## V. RESULTS AT 900 MHz

### A. Dipole Configurations

The position of the dipole in the above-mentioned absorption studies [9]–[11] was chosen because it results in the largest absorption. The brain was also considered to be the most relevant tissue with respect to health-risk considerations. Another reason for choosing the position was its rather simple and well-defined tissue distribution, i.e., small shifts parallel to the surface of the skin do not result in significant changes of the absorption pattern. Much larger variation must be expected for the ear region, which is composed of a complex 3-D tissue distribution, including air cavities and low-loss bone structures, as well as various wet tissues.

The basic investigation on the absorption in the ear region was also performed using the dipole since it has a well-defined current distribution, which does not strongly depend on the load, i.e., on the scattered field. The effect on the impedance, which would significantly distort the evaluation of the absorption in the ear as a function of the modeling, can be avoided by normalizing all values to a constant feedpoint current of 100 mA. The vertical dipole was shifted on a matrix parallel to the head surface, with a distance to the closest tissue voxel of 2 mm for the inhomogeneous phantom. The separation of the $3 \times 3$ matrix was 20 mm in the $z$- and 15 mm in the $y$-direction. The values were compared to those of the homogeneous phantom (HTSL1: $\epsilon_{r1} = 43.5$, $\sigma_1 = 0.9$ mho/m) with a 4-mm lossless spacing. The dielectric parameters were chosen from [21] (Table II), which are more recent than the dielectric parameters used in the previous studies.

The results of a representative position directly behind the opening of the auditory canal is shown in Fig. 8, in which the two additional distances of 5 and 10 mm were also evaluated in order to verify whether the findings have a strong distance dependence.

At this particular position, the earlier assumption holds that filling the low-loss structure of the inner ear with lossy liquid compensates for the losses in the pinna (Fig. 9). However, the

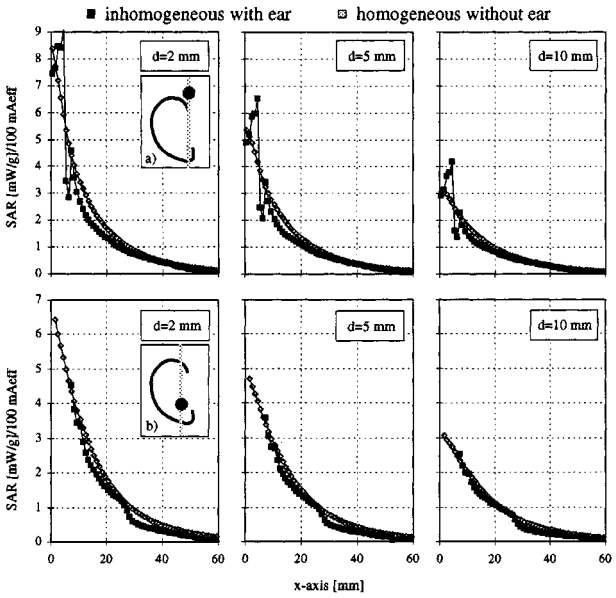


Fig. 8. SAR distribution along a line perpendicular to the 0.45-$\lambda$ (900-MHz) dipole axis. a) 5 mm above the pinna (top. b) Directly behind the feedpoint (bottom). The dipole was positioned with its feedpoint directly behind the opening of the auditory canal at three distances (2/5/10 mm) to the outermost voxel of the pinna. The dot in a) and b) corresponds to the position of the axis where the SAR was evaluated. In a) and b), anatomically correct modeling including the complicated shaped ear region is compared to homogeneous modeling (HTSL1: $\epsilon_{r1} = 43.5$, $\sigma_1 = 0.9$ mho/m) without an ear and a simplified ear region.

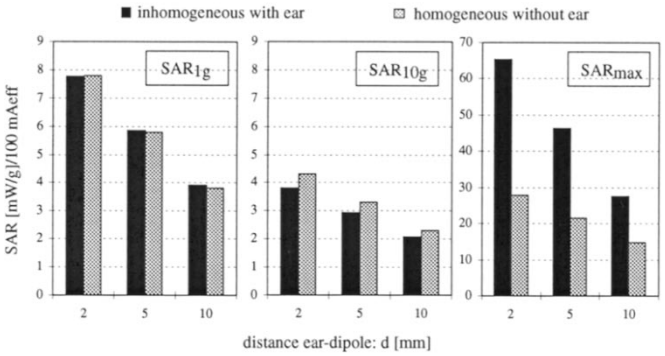


Fig. 9. Spatial-peak SAR values averaged over 1 and 10 g and the maximum one-voxel SAR for the 0.45-$\lambda$ dipole (900 MHz) located with its feedpoint at the opening of the auditory canal for the inhomogeneous phantom including the ear as well as for the homogeneous phantom (HTSL1: $\epsilon_{r1} = 43.5$, $\sigma_1 = 0.9$ mho/m) without ear but with a 4 mm spacer.

volume containing the spatial-peak SAR value shifts away from the feedpoint to areas of greater wet tissue content. This is represented in Fig. 10, showing a shift in position of the averaging volume to outside the complex-shaped air-containing ear region for inhomogeneous modeling. Since the homogeneous phantom shall be designed to well represent the spatial-peak SAR values, the homogeneous head without the ear will not well represent the local-peak SAR, which occurs in the pinna (Fig. 8). It must also be noted that these local values strongly depend on the shape of the ear. On the other hand such single-voxel based values incorporate large uncertainties due to numerical artifacts, which can easily exceed 100% [15].

Based on these results, considerably larger spatial-peak SAR values had to be expected when the feedpoint of the dipole is

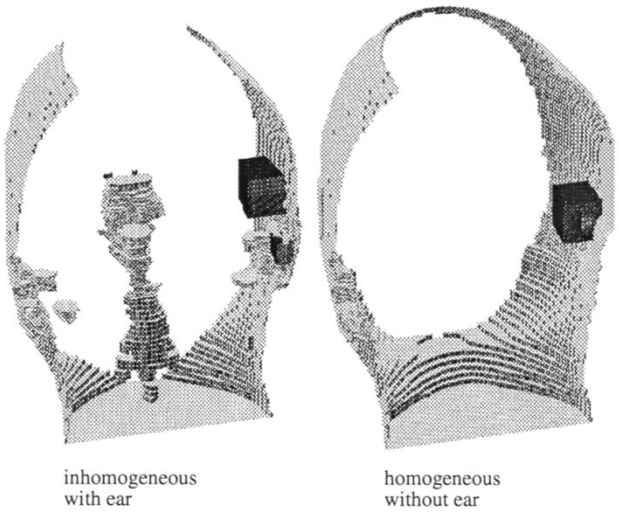


Fig. 10. Locations of the 1- and 10-g averaging volumes in the human head model are shown for inhomogeneous modeling (left-hand side) and homogeneous modeling (right-hand side) for a 0.45-$\lambda$ dipole. The feedpoint is located directly behind the auditory canal; the distance between the dipole and the closest voxel is 2 mm. For homogeneous modeling, the 1-g cube is located inside the 10-g cube.

shifted to locations where the tissue volume of the pinna in the proximity of the feedpoint is considerably larger. To study this dependence, the dipole's position was shifted on a plane parallel to the ear on a $3 \times 3$ matrix, the results of which are plotted in (Fig. 11). The largest spatial-peak SAR (1-g averaged) was approximately 3 dB above the value found at the center position. The reason is the larger volume of the pinna and that the bone structure of the inner ear does not entirely extend to this ear region. However, this dipole simulates a concentrated source within only 2 mm from the tissue, which is unlikely to occur in daily situations.

### *B. Generic Phone Configuration in Simplified Positions*

In order to better represent the actual exposure with a more distributed source in the area of the ear, a generic phone with dimensions as represented in Fig. 3 has been used in the following studies. It consists of a simple box with a monopole antenna of realistic dimensions. In order to compare our results with the findings of previous studies, the phone was first positioned vertically (position $B1$) and horizontally (position $B2$) next to the ear (90° with respect to the line connecting both auditory canals). The reason that this rather uncommon position was favored by most studies was the shortcoming of most numerical tools in the support of tilting head models without significantly impairing modeling accuracy.

The distance to the closest voxel of the pinna was, in both positions, 2 mm in order to account for the thickness of the synthetic material around the device body. The location of the imaginary loudspeaker was directly behind the opening of the auditory canal, as represented in Fig. 3. For the homogeneous phantom (HTSL1: $\epsilon_{r1} = 43.5$, $\sigma_1 = 0.9$ mho/m) a lossless spacer of 4 mm (i.e., 6 mm between the surface of the phantom's skin and the metallic box) and 6 mm (8 mm, respectively) was chosen. The results for the 1- and 10-g values for positions $B1$ and $B2$ are summarized in Fig. 12. It becomes obvious that a

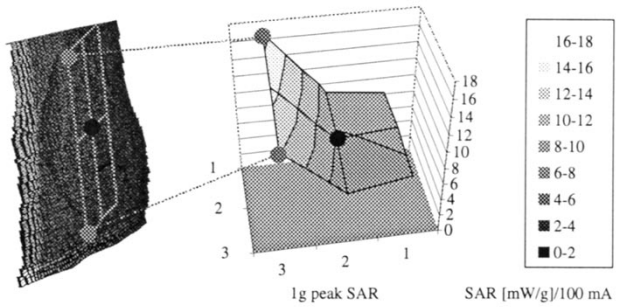


Fig. 11. Spatial-peak SAR values (right) averaged over 1 g for the 0.45 $\lambda$ dipole (900 MHz) located with its feedpoint at nine different locations on a plane parallel to the ear (left-hand side). The middle position (black dot) corresponds to the position described in Figs. 8 and 7.

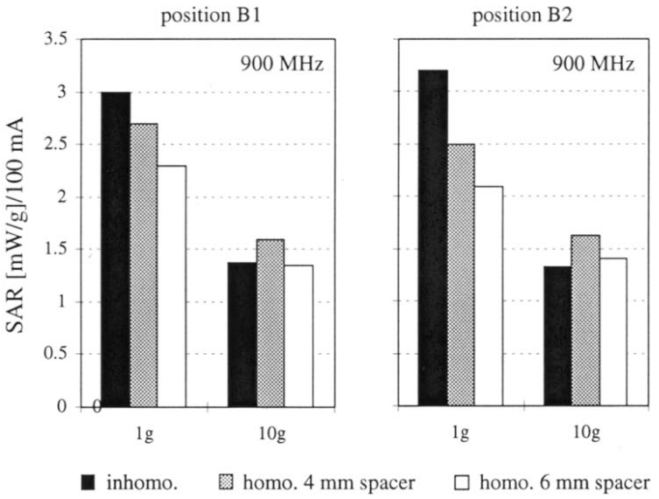


Fig. 12. Spatial-peak SAR values averaged over 1- and 10-g for vertical $B1$ (left-hand side) and horizontal $B2$ (right-hand side) phone positions for the inhomogeneous phantom including the ear, as well as for the homogeneous phantom (HTSL1: $\epsilon_{r1} = 43.5$, $\sigma_1 = 0.9$ mho/m) without the ear, but with a 4/6-mm spacer at 900 MHz.

spacer of 3–4 mm represents the maximum exposure of the inhomogeneous phantom much better than a spacer of 6 mm. As expected, the spatial-peak SAR values averaged over a cube of 10 g are much less sensitive to the location of the phone and modeling of the ear.

### *C. Intended Use Position*

To verify these findings for more realistic positions with respect to the head, the dipole and phone were evaluated in a position that corresponds to the intended use position defined by [2]. In the first step, the CAD data of the head was rotated by 23° around its $x$-axis and $-7°$ around its $z$-axis (Fig. 2), which represents the intended use position (position $B3$). The CAD model of the dipole or phone was added and a new graded mesh aligned to the coordinate system of the source was then generated (Fig. 13). This procedure results in a discretization that neither adds uncertainties to the phone modeling, nor changes the accuracy of the head modeling compared to the previous positions.

The spatial-peak SAR values averaged over 1 and 10 g are represented in Fig. 14 for the dipole and in Fig. 13 for the generic

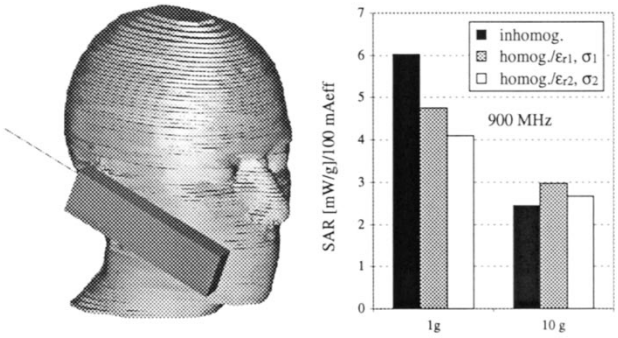


Fig. 13. Rotated head (left-hand side) and spatial-peak SAR values averaged over 1 and 10 g for an intended use position of the generic phone (position $B3$) for homogeneous (HTSL1: $\epsilon_{r1} = 43.5$, $\sigma_1 = 0.9$ mho/m and HTSL2: $\epsilon_{r2} = 45.8$, $\sigma_2 = 0.77$ mho/m) and inhomogeneous modeling at 900 MHz.

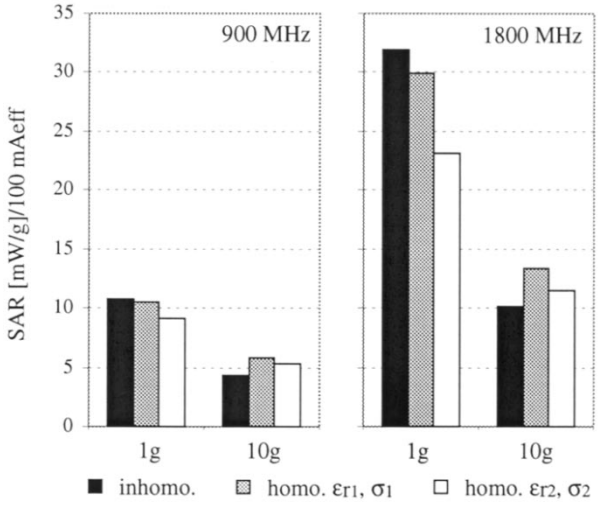


Fig. 14. Dipole configuration with a rotated head in position $B3$ and spatial-peak SAR values averaged over 1 and 10 g for a 0.45-$\lambda$ dipole at 900 (left-hand side) and 1800 MHz (right-hand side). The closest distance between the dipole and head is 4 mm. The dielectric parameters for the homogeneous phantoms are HTSL1: $\epsilon_{r1} = 43.5$, $\sigma_1 = 0.9$ mho/m and HTSL2: $\epsilon_{r2} = 45.8$, $\sigma_2 = 0.77$ mho/m at 900 MHz, HTSL1: $\epsilon_{r1} = 41$, $\sigma_1 = 1.69$ mho/m and HTSL2: $\epsilon_{r2} = 43.5$, $\sigma_2 = 1.15$ mho/m at 1800 MHz

phone for a 4-mm lossless spacer. As for the previous position, the maximum underestimation exposure for the investigated source with homogeneous modeling without an ear, using a spacing of 4 mm and dielectric parameter set of HTSL1 was 20% for the 1-g spatially averaged SAR. Using the dielectric parameter set of HTSL2, the underestimation was more pronounced (30%).

## VI. Results at 1800 MHz

Additional studies were necessary at 1800 MHz since it is not, *per se*, obvious that the findings are also valid at higher frequencies due to the significantly reduced skin depth. It is expected that a larger amount of the total energy loss is absorbed in the external ear and skin. For comparison, the homogeneous phantom was simulated with both dielectric parameter sets HTSL1 and HTSL2.

The results are summarized in Figs. 14 and 15, from which similar conclusions at 900 MHz can be drawn under the condition that the homogeneous phantom is modeled with the dielectric parameter set of HTSL1. Employing the dielectric parameter set of HTSL2, the underestimation is quite significant, suggesting that the thickness of the spacer must either be reduced or the ear must be modeled by a lossy cartilage-like material.

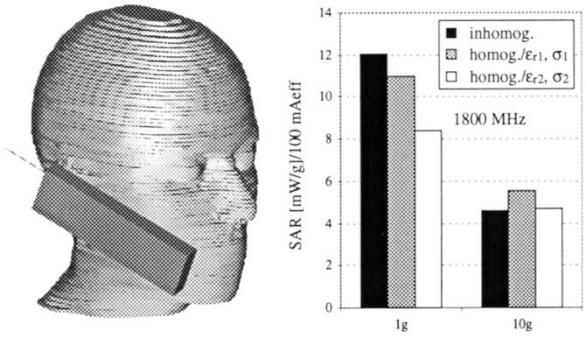


Fig. 15. Rotated head (left-hand side) and spatial-peak SAR values averaged over 1 and 10 g for an intended use position of the generic phone (position $B3$) for homogeneous (HTSL1: $\epsilon_{r1} = 41$, $\sigma_1 = 1.69$ mho/m and HTSL2: $\epsilon_{r2} = 43.5$, $\sigma_2 = 1.15$ mho/m) and inhomogeneous modeling at 1800 MHz.

## VII. Discussion and Conclusions

This paper on the exposure of the ear was based on one particular phantom only, i.e., it does not provide information about the variations of different ears. In addition, the exposure was only investigated for two generic transmitters. Nevertheless, the study enables conclusions to be made that are generally valid within reasonable limits.

The basic requirement for a sound procedure shall enable demonstration of compliance for a reasonable cross section of users. This ultimately requires simplifications, since the absorption significantly depends on the internal and external anatomy of the user. The simplification is driven by the requirement to define a single phantom that satisfies the following criteria: the exposure assessed with this phantom for a given MTE and position shall not underestimate the actual maximum exposure occurring in a reasonable cross section of users. Based on the previous studies, it was shown that this is possible with a homogeneous head of appropriate shape and dielectric parameters despite the considerable anatomical variations. This had been validated with the exception of the ear region. The ear region is of special complexity with respect to absorption because of the complex structure of the inner ear and the considerable anatomical variations in shape, size, and thickness of the external ear. In addition, the external ear is always in direct contact with the device. On the other hand, the external ear has proven to be quite resistant to all kinds of chemical and physical agents, as well as environmental stress. However, current safety guidelines do not define different safety limits for the external ear.

The results of this paper suggest that, for this particular person, the spatial-peak exposure in the ear region can be appropriately modeled by simulating the head homogeneously by selecting the dielectric parameter set of HTSL1 and simulating the ear pinna by a lossless spacer of 3–4-mm thickness. Using a 4-mm spacer, the maximum underestimation of the spatially 1-g averaged peak SAR using a generic phone as a source was below 20%. The 10-g averaged spatial-peak SAR, however, was never underestimated. In case of a worst-case exposure

source, the underestimation of the 1-g averaged value could be as high as 3 dB.

To obtain a more comprehensive database valid for a reasonable cross section of the user group, a larger number of human head models, including realistically modeled ears, would have to be analyzed in a similarly detailed approach as presented herein. This would clearly exceed the resources of our laboratory. Nevertheless, since the head phantom used has no obvious significant deviation from a normal head, it is unlikely that using other head phantoms will significantly change the basic findings of this paper. Consequently, this paper permits the general conclusion that a lossless spacer of $>4$ mm would result in significant underestimation of some exposures. On the other hand, a very thin spacer would overestimate the exposure in the area above the ear. Consequently, a rigorous approach fully complying with the results of this paper would be to model the extension of the outer ear sufficiently large (e.g., 90% percentile) and the thickness of the compressed ear correspondingly thin (e.g., 10% percentile), whereby the ear should be partially filled with tissue simulating liquid by providing a minimum distance between the device and liquid of not larger than 3 mm.

## ACKNOWLEDGMENT

The authors gratefully acknowledge the support of Prof. P. Bösiger, Laboratory of Biomedical Engineering, and Dr. D. Müller, Laboratory of Biomedical Engineering, for obtaining the MRI data, the performance of the measurements by K. Poković, the advice and help of Dr. E. Kühn, Dr. B. Eicher, Dr. L. Martens, and Dr. C. Gabriel, as well as the editing of this paper's manuscript by M. Stubbs.

## REFERENCES

[1] "Evaluating compliance with FCC guidelines for human exposure to radio frequency electromagnetic fields," Fed. Commun. Commission, Washington, DC, 20 554 Tech. Rep. OET Bull. 65, 1997.

[2] "Considerations for evaluation of human exposure to Electromagnetic Fields (EMF's) from Mobile Telecommunication Equipment (MTE) in the frequency range 30 MHz–6 GHz," CENELEC, Brussels, Belgium, prES 59005, CLC/TC211 (SEC) 17, Mar. 1998.

[3] *Specific Absorption Rate (SAR) Estimation for Cellular Phone*, ARIB STD-T56, Jan. 1998.

[4] T. Schmid, O. Egger, and N. Kuster, "Automated $E$-field scanning system for dosimetric assessments," *IEEE Trans. Microwave Theory Tech.*, vol. 44, pp. 105–113, Jan. 1996.

[5] C. Gabriel, "Phantom models for antenna design and exposure assessment," in *IEE Colloq. Design of Mobile Antennas for Optimal Performance in Presence of Biolog. Tissue*, Jan. 1997.

[6] Q. Balzano, O. Garay, and T. J. Manning, "Electromagnetic energy exposure of simulated users of portable cellular telephones," *IEEE Trans. Veh. Technol.*, vol. 44, pp. 390–403, Aug. 1995.

[7] N. Kuster, R. Kästle, and T. Schmid, "Dosimetric evaluation of handheld mobile communications equipment with known precision," *IEICE Trans. Commun.*, vol. 80, no. 5, pp. 645–652, May 1997.

[8] N. Kuster and Q. Balzano, "Energy absorption mechanism by biological bodies in the near field of dipole antennas above 300 MHz," *IEEE Trans. Veh. Technol.*, vol. 41, pp. 17–23, Feb. 1992.

[9] V. Hombach, K. Meier, M. Burkhardt, E. Kühn, and N. Kuster, "The dependence of EM energy absorption upon human head modeling at 900 MHz," *IEEE Trans. Microwave Theory Tech.*, vol. 44, pp. 1855–1863, Oct. 1996.

[10] K. Meier, V. Hombach, R. Kästle, R. Y-S. Tay, and N. Kuster, "The dependence of electromagnetic energy absorption upon human-head modeling at 1800 MHz," *IEEE Trans. Microwave Theory Tech.*, vol. 45, pp. 2058–2062, Nov. 1997.

[11] F. Schoenborn, M. Burkhardt, and N. Kuster, "Differences in energy absorption between heads of adults and children in the near field of sources," *Health Phys.*, vol. 74, no. 2, pp. 160–168, 1998.

[12] P. J. Dimbylow and S. M. Mann, "SAR calculations in an anatomically realistic model of the head for mobile communication transceivers at 900 MHz and 1.8 GHz," *Phys. Med. Biol.*, vol. 39, pp. 1537–1553, 1994.

[13] T. Hamada, S. Watanabe, and M. Taki, "Effect of pinna on the local ears in a human head exposed to microwave," in *20th Annu. Bioelectromag. Soc. Meeting*, Saint Petersburg, FL, June 1998, p. 99.

[14] O. P. Gandhi, G. Lazzi, and C. M. Furse, "Electromagnetic absorption in the human head and neck for mobile telephones at 835 and 1900 MHz," *IEEE Trans. Microwave Theory Tech.*, vol. 44, pp. 1884–1897, Oct. 1996.

[15] M. Burkhardt and N. Kuster, "Artifacts at material boundaries of lossy dielectric bodies in FDTD simulations," in *IEEE Antennas Propagat. Symp.*, Atlanta, GA, June 1998, p. 72.

[16] A. Taflove, *Computational Electromagnetics: The Finite-Difference Time-Domain Method*. Norwood, MA: Artech House, 1995.

[17] *The MAFIA Collaboration, Mafia Version 3.x, User's Guide CST GmbH*, CST, Darmstadt, Germany, 1994.

[18] T. Weiland, "Maxwell's grid equations," *Frequenz*, vol. 44, no. 1, pp. 9–16, 1990.

[19] N. Buechler, D. H. Roper, C. H. Durney, and D. A. Christensen, "Modeling sources in the FDTD formulation and their use in quantifying source and boundary condition errors," *IEEE Trans. Microwave Theory Tech.*, vol. 43, pp. 810–813, Apr. 1995.

[20] C. Gabriel, *Dielectric Database*. London, U.K.: Microwave Consultants Ltd., 1994.

[21] ——, "Compilation of the Dielectric Properties of Body Tissues at RF and Microwave Frequencies," Brooks Air Force Base, Brooks AFB, TX, Tech. Rep. AL/OE-TR-1996-0037, 1996.

**Michael Burkhardt** (M'95–M'99) was born in Ludwigshafen, Germany, in March 1969. He received the Diploma degree in electrical engineering from the Technical University of Darmstadt, Darmstadt, Germany, in 1995, and the Ph.D. degree from the Swiss Federal Institute of Technology, Zurich, Switzerland, in 1999. His thesis was devoted to uncertainty assessments in computational electrodynamics.

From October 1994 to May 1995, he was with the Institute National Polytechnique de Grenoble, Grenoble, France. In October 1999, he joined diAx, Zurich, Switzerland, which is a GSM/DCS service provider, and is currently with the Regulatory Group.

**Niels Kuster** (M'93) was born in Olten, Switzerland, in June 1957. He received the Diploma and Ph.D. degrees in electrical engineering from the Swiss Federal Institute of Technology (ETH), Zurich, Switzerland.

In 1985, he joined the Electromagnetics Laboratory, ETH, where he was involved in research and development of the generalized multipole technique (GMT) and the 3-D MMP code. In 1992, he was an invited Professor at Motorola Inc., Fort Lauderdale, FL, for a trimester. He is currently a Professor in the Department of Electrical Engineering, ETH, and the Designated Director of the Foundation for Research on Information Technologies in Society (IT'IS), Zurich, Switzerland. His research interests include all aspects of numerical techniques in electrodynamics, near-field measurement techniques, antenna design and the biological effects of electromagnetic fields. He is a member of various scientific societies and official member of the URSI Commission K.